Available online at www.sciencedirect.com

ScienceDirect

Ceramics International 40 (2014) 3873–3878

CERAMICS INTERNATIONAL

www.elsevier.com/locate/ceramint

Negative thermal expansion and shift in phase transition temperature in Mo-substituted ZrW_2O_8 thin films prepared by pulsed laser deposition

Hongfei Liu[a,*], Kunmin Pan[a], Qu Jin[a], Zhiping Zhang[b], Gang Wang[a], Xianghua Zeng[a]

[a]School of Physics Science and Technology, Yangzhou University, Yangzhou 225002, PR China
[b]Department of Electrical and Mechanical Engineering, Guangling College, Yangzhou University, Yangzhou 225002, PR China

Received 21 July 2013; received in revised form 6 August 2013; accepted 6 August 2013
Available online 14 August 2013

Abstract

Mo-substituted ZrW_2O_8 ($ZrW_{1.1}Mo_{0.9}O_8$) thin films have been deposited on quartz substrates by the pulsed laser deposition (PLD) method. The effects of oxygen pressure, substrate temperature and annealing temperature on the morphologies and phase compositions of the $ZrW_{1.1}Mo_{0.9}O_8$ thin films were systematically investigated using X-ray diffraction (XRD) and scanning electron microscope (SEM). The negative thermal expansion and shift in phase transition temperature in cubic $ZrW_{1.1}Mo_{0.9}O_8$ thin films were characterized using high temperature X-ray diffraction. The results indicate that as-deposited $ZrW_{1.1}Mo_{0.9}O_8$ thin films show amorphous phases. Crystallized cubic $ZrW_{1.1}Mo_{0.9}O_8$ thin films were prepared by heating at 1050 °C for 7 min. The growth of the $ZrW_{1.1}Mo_{0.9}O_8$ thin films was strongly influenced by the substrate temperature and oxygen pressure. The $ZrW_{1.1}Mo_{0.9}O_8$ thin film deposited at 500 °C with an oxygen pressure of 10 Pa was smooth and compact, and its thickness was about 720 nm. The high temperature X-ray diffraction analyses demonstrated that the cubic $ZrW_{1.1}Mo_{0.9}O_8$ thin film exhibited strong negative thermal expansion and its thermal expansion coefficient was calculated to be $-8.65\times10^{-6}\,K^{-1}$ from 100 °C to 600 °C. The substitution of Mo in ZrW_2O_8 thin film leads to a remarkable decrease in phase transition temperature, with the α to β structure phase transition occurring below 100 °C. However, with increased testing temperature, the substitution results in part of the cubic $ZrW_{1.1}Mo_{0.9}O_8$ thin film gradually changing into a trigonal phase.

Keywords: Negative thermal expansion; Phase transition; Thin film; Pulsed laser deposition

1. Introduction

Negative thermal expansion ZrW_2O_8 thin films have attracted much interest due to their important applications in optics, microelectronics, and thermally sensitive mechanical devices [1–7]. They can be used as fillers to tailor the thermal expansion coefficients of functional surface coating layers and thin films to avoid problems caused by mismatches in thermal expansion coefficients between layered films and base materials at various working temperatures, such as coating delamination, mechanical destruction and positional deviation [8–12].

In our earlier work, pure ZrW_2O_8 thin films were successfully prepared on quartz substrates by the pulsed laser deposition (PLD) method for the first time, and the ZrW_2O_8 thin films showed strong negative thermal expansion. However, it was found that the cubic ZrW_2O_8 thin film undergoes a phase transition from α-ZrW_2O_8 to β-ZrW_2O_8 between 100 °C and 200 °C [13–15]. This phenomenon was also found in ZrW_2O_8 powders and ceramics between 150 °C and 160 °C. This phase transition leads to a remarkable deviation from the linear temperature dependence of the expansion coefficient from $-9.0\times10^{-6}\,K^{-1}$ to $-6.0\times10^{-6}\,K^{-1}$[1–2]. The abrupt change of thermal expansion is disadvantageous for potential applications if the phase transition temperature (Tc) is within the working temperature range. The ability to adjust the phase transition temperature could therefore be of great practical importance if it allows the temperature of the phase transition to be moved out of the practical working range of the materials.

In this work, in order to shift the phase transition temperature of the cubic ZrW_2O_8 thin film, Mo-substituted ZrW_2O_8 ($ZrW_{1.1}Mo_{0.9}O_8$) thin films were synthesized by the pulsed

*Corresponding author. Tel.: +86 514 87975466; fax: +86 514 87975467.
E-mail address: liuhf@yzu.edu.cn (H. Liu).

0272-8842/$ - see front matter © 2013 Elsevier Ltd and Techna Group S.r.l. All rights reserved.
http://dx.doi.org/10.1016/j.ceramint.2013.08.028

laser deposition (PLD) method. PLD is a versatile fabrication technique that enables preservation of target stoichiometry while producing high-quality thin films. The magnitude of negative thermal expansion and phase transition temperature in resulting $ZrW_{1.1}Mo_{0.9}O_8$ thin films were investigated, and the effect of annealing temperature, oxygen pressure and substrate temperature on the morphology and phase composition of the $ZrW_{1.1}Mo_{0.9}O_8$ thin films was also characterized.

2. Experimental procedure

The $ZrW_{1.1}Mo_{0.9}O_8$ ceramic target was prepared by a co-precipitation route using $H_{40}N_{10}O_{41}W_{12}\cdot xH_2O$ ($\geq 99.95\%$), $N_6H_{24}Mo_7O_{24}\cdot 4H_2O$ ($\geq 99.95\%$) and $ZrO(NO_3)_2\cdot 5H_2O$ ($\geq 99.95\%$) as raw materials [13], which were dissolved separately in distilled water according to the molar ratio of Zr:W:Mo = 1:1.1:0.9. The Zr solution was added slowly to the mixture of W and Mo solution dropwise with constant stirring at about 70 °C. After stirring over 2 h, the precursors were filtered, dried at 80 °C, and subsequently calcined at 600 °C for 4 h. Next, the powders were pressed and calcined at 1050 °C for 3 h in air, then quenched in de-ionized water to obtain the $ZrW_{1.1}Mo_{0.9}O_8$ ceramic target. The $ZrW_{1.1}Mo_{0.9}O_8$ ceramic target was polished and cleaned before placing into the vacuum chamber.

Thin films were grown on quartz substrates by PLD method using a KrF excimer pulsed laser with a wavelength of 248 nm. The substrates were placed into the vacuum chamber with a base pressure of 5.0×10^{-4} Pa. The distance between target and substrate was about 3.5 cm. The laser flux approximately was 356 mJ/cm^2 and the repetition rate was 5 Hz. During deposition, oxygen was introduced into the chamber and kept at a constant pressure between 5 and 20 Pa while depositing. The deposition time was 50 min. The deposition temperature of the film was room temperature, 300 °C or 500 °C, respectively. After deposition, the as-deposited films were post-annealed at 1050 °C for better crystallization.

Phase identification and structural characterization were carried out using an XRD Rigaku D/max 2500 with CuKα radiation. Data were collected at 40 kV and 200 mA, with a scanning speed of 5°/min over an angular range of 10°–60°, High temperature X-ray diffraction data were also collected on the XRD Rigaku D/max 2500. HTXRD patterns for the resulting cubic $ZrW_{1.1}Mo_{0.9}O_8$ thin films were collected in air at 20 °C, 100 °C, 150 °C, 200 °C, 300 °C, 400 °C, 500 °C and 600 °C. The heating rate was set at 5 °C/min, and the samples were annealed for 10 min at each testing temperature before collecting the XRD data. Surface morphologies and thicknesses of the as-deposited $ZrW_{1.1}Mo_{0.9}O_8$ thin films and annealed thin films were studied with a Hitachi S-4800 field emission scanning electron microscope (FESEM).

3. Results and discussion

Fig.1 shows the XRD patterns of the $ZrW_{1.1}Mo_{0.9}O_8$ precursors calcined at 600 °C and 1050 °C. When the $ZrW_{1.1}Mo_{0.9}O_8$ precursors were calcined at 600 °C (Fig. 1(a)), some reflections of WO_3 (JCPDS 43-1035), ZrO_2 (JCPDS 65-1025) and trignoal $ZrW_{1.1}Mo_{0.9}O_8$ were present. When the precursors were calcined at 1050 °C for 7 h and then quenched in deionized water, the cubic $ZrW_{1.1}Mo_{0.9}O_8$ target was obtained, and the XRD pattern of the resulting cubic $ZrW_{1.1}Mo_{0.9}O_8$ target is shown in Fig. 1(b). However, a small amount of residual ZrO_2 was detected. This is mainly due to the volatility of MoO_3 and WO_3. It was also found that the color of the surface layer of $ZrW_{1.1}Mo_{0.9}O_8$ target was different from the interior of the target. The surface layer of the $ZrW_{1.1}Mo_{0.9}O_8$ target was very thin. When the obtained $ZrW_{1.1}Mo_{0.9}O_8$ target was polished, the XRD pattern of the interior part of the $ZrW_{1.1}Mo_{0.9}O_8$ target did not indicate the presence of a ZrO_2 phase, as shown in Fig. 1(c). All diffraction peaks were accounted for by the cubic unit cell of α-ZrW_2O_8 (JCPDS #50-1868) which indicates that the resulting $ZrW_{1.1}Mo_{0.9}O_8$ target is pure (Fig. 1(c)).

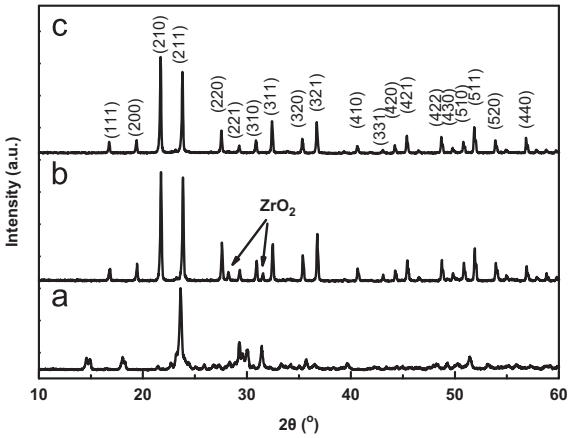

Fig. 1. XRD patterns of the $ZrW_{1.1}Mo_{0.9}O_8$ precursors sintered at different temperatures (a) 600 °C for 3 h; (b) 1050 °C for 7 h and then quenched in deionized water (before polishing); and (c) 1050 °C for 7 h and then quenched in deionized water (after polishing).

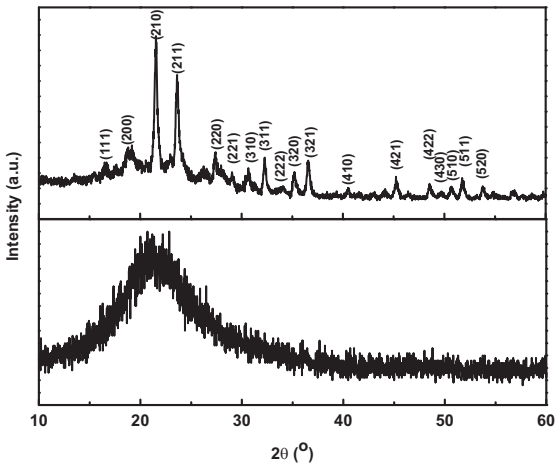

Fig. 2. XRD patterns of the $ZrW_{1.1}Mo_{0.9}O_8$ thin film (a) as-deposited and (b) post-deposition annealed at 1050 °C.

Room temperature XRD patterns of as-deposited and annealed $ZrW_{1.1}Mo_{0.9}O_8$ films are shown in Fig. 2. All XRD patterns of as-deposited $ZrW_{1.1}Mo_{0.9}O_8$ thin films are

amorphous (Fig. 2(a)) regardless of O_2 pressures and substrate temperatures. This is a common observation in compound sputtering, where the components in the compound may differ from each other in preferred crystal structure, lattice constants and chemical properties. The interaction of different components greatly inhibits the diffusion of the atoms, which results in an increased likelihood of forming amorphous phases in compound sputtering [15]. When the high-energy particles impinge on the substrate at low temperature, they do not have adequate time and energy to diffuse. Thus post deposition annealing is needed to induce crystallization, and XRD analysis shows that the film crystallinity is dependent on

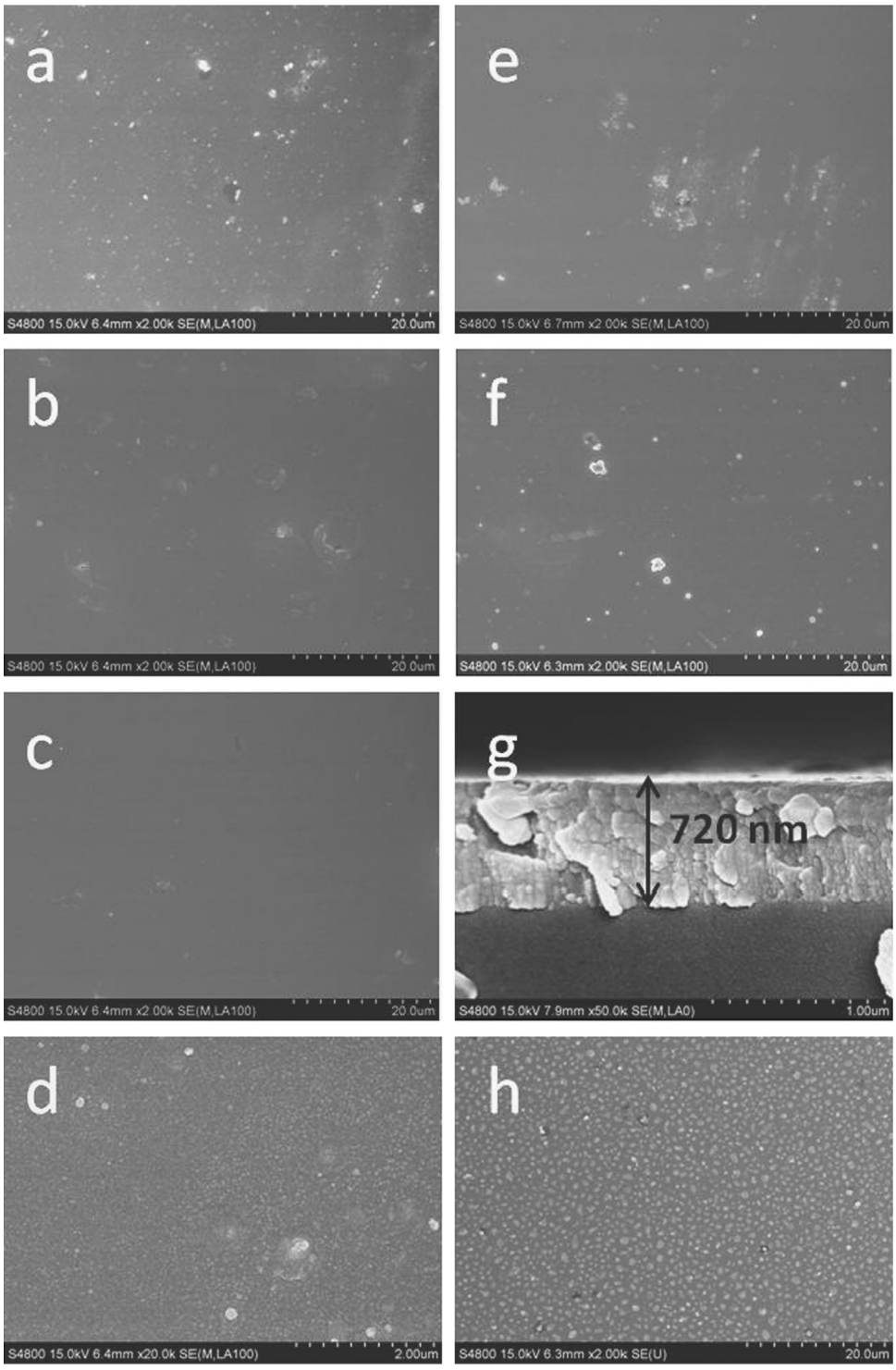

Fig. 3. SEM images of the $ZrW_{1.1}Mo_{0.9}O_8$ thin films grown on quartz substrates at different conditions (a) 10 Pa and without heating; (b) 10 Pa and 300 °C; (c) 10 Pa and 500 °C; (d) 10 Pa and 500 °C (high resolution image); (e) 5 Pa and 500 °C; (f) 20 Pa and 500 °C; (g) Cross sectional SEM image of $ZrW_{1.1}Mo_{0.9}O_8$ thin film deposited at the oxygen pressure of 10 Pa and substrate temperature of 500 °C; and (h) post-deposition annealed at 1050 °C for 7 min.

post-deposition annealing temperatures. Annealing an as-deposited $ZrW_{1.1}Mo_{0.9}O_8$ thin film at 1050 °C for 7 min followed by quenching in distilled water, gave a phase pure cubic $ZrW_{1.1}Mo_{0.9}O_8$ thin film (Fig. 2b). By comparison with the $ZrW_{1.1}Mo_{0.9}O_8$ target in Fig. 1(c), it is shown that there are no impurity peaks in the XRD pattern.

Fig. 3 shows the surface morphologies of the $ZrW_{1.1}Mo_{0.9}O_8$ thin films prepared under different conditions. The surface morphologies of $ZrW_{1.1}Mo_{0.9}O_8$ thin films are strongly dependent on the substrate temperature when the oxygen pressure and laser energy are fixed [17,18]. Fig. 3 shows the surface morphologies of $ZrW_{1.1}Mo_{0.9}O_8$ thin films deposited at different substrate temperatures. Room temperature deposition results in the formation of distinct particles. This is mainly because the particles do not have adequate energy to diffuse. As a result, lots of particles appear. The surface morphology changes with substrate temperature (Fig. 3(b) and (c)), with increasing substrate temperature, the particles almost disappear. When the $ZrW_{1.1}Mo_{0.9}O_8$ thin film was deposited on quartz substrates at 300 °C, the quality of the thin film was enhanced, but there were still some defects. When the $ZrW_{1.1}Mo_{0.9}O_8$ thin film was deposited at 500 °C, the thin film was smooth and compact (see Fig. 3(c)), and the surface of the film did not show significant grain growth, which also indicates the amorphous state of the thin film. Fig. 3(d) is a high resolution image of Fig. 3(c), which shows the as-deposited $ZrW_{1.1}Mo_{0.9}O_8$ thin film is composed of nanoparticles.

The oxygen partial pressure also has a large effect on the surface morphologies of the films. Fig. 3(e), (c) and (f) shows SEM images of $ZrW_{1.1}Mo_{0.9}O_8$ thin films deposited at oxygen pressures of 5 Pa, 10 Pa and 20 Pa. Intermediate oxygen pressures can improve the quality of $ZrW_{1.1}Mo_{0.9}O_8$ thin films. When the oxygen pressure reaches 20 Pa, collisions between atoms in the plasma plume and oxygen atoms are very strong, causing the surface mobility of adatoms to reduce significantly. Consequently, a number of defects are formed (Fig. 3f). When the oxygen pressure was 5 Pa, some particles were visible in the micrograph of the $ZrW_{1.1}Mo_{0.9}O_8$ thin film (Fig. 3(e)). The $ZrW_{1.1}Mo_{0.9}O_8$ thin film deposited at an oxygen pressure of 10 Pa is most smooth and compact. It is mainly because the atoms gain an appropriate energy by scattering of oxygen atoms, which prompts the adatoms to

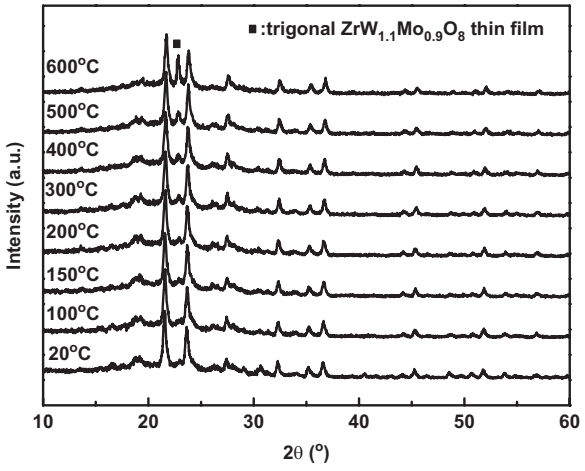

Fig. 4. XRD patterns of the cubic $ZrW_{1.1}Mo_{0.9}O_8$ thin film collected at different temperatures.

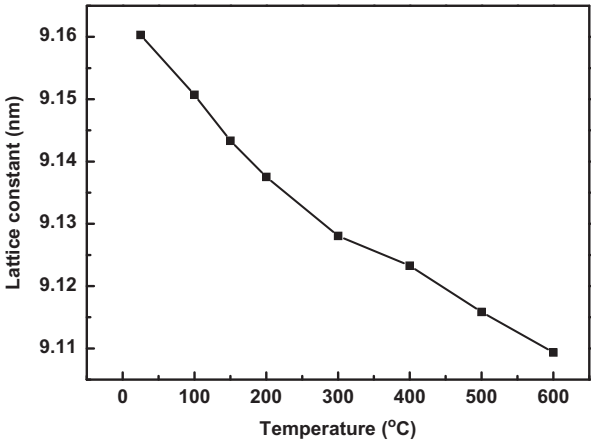

Fig. 6. The lattice constant dependence on temperature for the cubic $ZrW_{1.1}Mo_{0.9}O_8$ thin film.

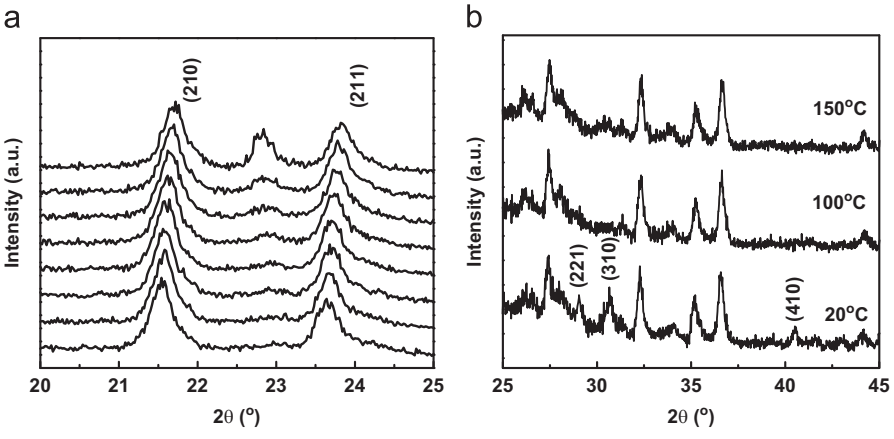

Fig. 5. Sections of the XRD patterns of the cubic $ZrW_{1.1}Mo_{0.9}O_8$ thin film (a) XRD patterns of the 210 peak and 211 peak of the cubic $ZrW_{1.1}Mo_{0.9}O_8$ thin film at different temperatures; and (b) sections of the XRD patterns of the cubic $ZrW_{1.1}Mo_{0.9}O_8$ thin film obtained at 25 °C, 100 °C and 150 °C.

reach thermodynamically stable locations through surface migration. Therefore, the thin film deposited at10 Pa shows a relatively flat surface [17–18]. Fig. 3(g) shows the cross-sectional FESEM image of the $ZrW_{1.1}Mo_{0.9}O_8$ thin film deposited under an oxygen pressure of 10 Pa on a quartz substrate at 500 °C, which has a thickness of about 720 nm. The SEM micrograph of the cubic $ZrW_{1.1}Mo_{0.9}O_8$ thin film annealed at 1050 °C for 7 min is shown in Fig. 3(h), which shows that the crystallized $ZrW_{1.1}Mo_{0.9}O_8$ thin film is poly-crystalline and many uniformly sized grains are formed.

XRD patterns of the resulting cubic $ZrW_{1.1}Mo_{0.9}O_8$ thin films were collected from 20 °C to 600 °C using in-situ high temperature XRD (Fig. 4). It can be seen that the entire XRD peaks of the cubic $ZrW_{1.1}Mo_{0.9}O_8$ thin film gradually shifts to higher 2θ as the testing temperatures increase (Fig. 5(a)). This is consistent with a decrease of the lattice constants and contraction of the cell volume of cubic $ZrW_{1.1}Mo_{0.9}O_8$. The lattice constants of the cubic $ZrW_{1.1}Mo_{0.9}O_8$ thin film at various temperatures were calculated by the cell parameter calculation method using the powder X software [19]. Fig. 6 shows the lattice constants of the cubic $ZrW_{1.1}Mo_{0.9}O_8$ thin film at various temperatures. The lattice constants decrease with increasing temperature, due to the negative thermal expansion of the obtained $ZrW_{1.1}Mo_{0.9}O_8$ thin film. The average linear thermal expansion coefficient of the cubic $ZrW_{1.1}Mo_{0.9}O_8$ thin film was calculated as -8.65×10^{-6} K^{-1} in the temperature range of 100–600 °C using linear regression. However, it was also found that part of the cubic $ZrW_{1.1}Mo_{0.9}O_8$ thin film gradually changed into trigonal $ZrW_{1.1}Mo_{0.9}O_8$ with increased testing temperatures (Fig. 4). This phenomenon was not observed in cubic ZrW_2O_8 thin films in our previous work [14,16], which indicates that the phase transformation from metastable cubic to stable trignal is caused by the substitution of Mo ions.

As shown in Fig. 5b, several XRD peaks of the cubic $ZrW_{1.1}Mo_{0.9}O_8$ thin film such as the (221), (310) and (410) peaks are present at 20 °C, but disappear at temperatures above 100 °C. In reports of cubic ZrW_2O_8 ceramics, the (221), (310) and (410) peaks are considered to be the indicators of the order-disorder-type phase transition, since these diffraction peaks disappear above the α to β structural phase transition temperature [19,20]. This indicates that a structural phase transition occurred in the cubic $ZrW_{1.1}Mo_{0.9}O_8$ thin film from α to β in the temperature range of 20–100 °C. In our previous work, the (221), (310) and (410) peaks of cubic ZrW_2O_8 thin film still existed at 100 °C, which indicated that the cubic ZrW_2O_8 thin film underwent an α to β structure phase transition between 100 °C and 200 °C. It was found that the structural phase transition temperature decreased with the introduction of Mo, which is similar to the Closmann's reports [21]. This is mainly due to the difference in bond strengths of Mo–O and W–O. With the introduction of the weaker Mo–O bond, the reversal of adjacent MO_4 tetrahedra becomes easier. The relationship between the substituted mass of Mo ions and the shift in phase transition temperature in $ZrW_{2-x}Mo_xO$ thin films will be discussed in detail in our future paper.

4. Conclusion

Cubic $ZrW_{1.1}Mo_{0.9}O_8$ thin films have been successfully prepared on quartz substrates by the PLD method using a $ZrW_{1.1}Mo_{0.9}O_8$ ceramic target after annealing at 1050 °C for 7 min. The resulting cubic $ZrW_{1.1}Mo_{0.9}O_8$ thin film shows excellent negative thermal expansion and its thermal expansion coefficient is calculated to be $-8.65\times10^{-6}\,K^{-1}$ from the100 °C to 600 °C. On the one hand, the substitution of Mo ions can effectively decrease the structural phase transition temperature, and the substitution also causes the cubic $ZrW_{1.1}Mo_{0.9}O_8$ thin film to gradually change into a trigonal phase with increasing testing temperatures.

Acknowledgments

The authors thank the Nation Natural Science Foundation of China (No. 51102207), the Yangzhou University Development Foundation for Talents (No. 0274640015427) and the Yangzhou University Science and Technique Innovation Foundation (No. 2010CXJ081).

References

[1] T.A. Mary, J.S.O. Evans, T. Vogt, A.W. Sleight, Negative thermal expansion from 0.3 K to 1050 K in ZrW_2O_8, Science 272 (1996) 90–92.
[2] S. Nishiiyama, T. Hayashi, T. Hattori, Synthesis of ZrW_2O_8 by quick cooling and measurement of negative thermal expansion of the sintered bodies, Journal of Alloys and Compounds 417 (2006) 187–189.
[3] N.A. Banek, H.I. Baiz, A. Latigo, C. Lind, Autohydration of nanosized cubic zirconium tungstate, Journal of the American Chemical Society 132 (2010) 8278–8279.
[4] H.F. Liu, Z.P. Zhang, W. Zhang, X.B. Chen, Effects of HCl concentration on the growth and negative thermal expansion property of the ZrW_2O_8 nanorods, Ceramics International 38 (2012) 1341–1345.
[5] K. Kanamori, T. Kineri, R. Fukuda, K. Nishio, A. Yasumori, Preparation and formation mechanism of ZrW_2O_8 by sol–gel process, Journal of the American Ceramic Society 90 (2008) 3542–3545.
[6] T. Varga, C. Lind, A.P. Wilkinson, H. Xu, C.E. Lesher, A. Navrotsky, Heats of formation for several crystalline polymorphs and pressure-induced amorphous forms of AMo_2O_8 (A=Zr, Hf) and ZrW_2O_8, Chemistry of Materials 19 (2007) 468–476.
[7] S. Nishiiyama, T. Hayashi, T. Hattori, Synthesis of ZrW_2O_8 by quick cooling and measurement of negative thermal expansion of the sintered bodies, Journal of Alloys and Compounds 417 (2006) 187–189.
[8] X.B. Yang, X.N. Cheng, X.H. Yan, J. Yang, T.B. Fu, J. Qiu, Synthesis of ZrO_2/ZrW_2O_8 composites with low thermal expansion, Composites Science and Technology 67 (2007) 1167–1171.
[9] P. Lommens, C.D. Meyer, E. Bruneel, K.D. Buysser, I.V. Driessche, S. Hoste, Synthesis and thermal expansion of ZrO_2/ZrW_2O_8 composites, Journal of the European Ceramic Society 25 (2005) 3605–3610.
[10] M.S. Sutton, J. Talghader, Zirconium tungstate (ZrW_2O_8)-based micro-machined negative thermal expansion thin films, Journal of Microelectromechanical Systems 13 (2004) 688–695.
[11] S. Yilmaz, D.C. Dunand, Finite-element analysis of thermal expansion and thermal mismatch stresses in a Cu-60 vol% ZrW_2O_8 composite, Composites Science and Technology 64 (2004) 1895–1898.
[12] S. Yilmaz, Thermal mismatch stress development in Cu-ZrW_2O_8 composite investigated by synchrotron X-ray diffraction, Composites Science and Technology 62 (14) (2002) 1835–1839.
[13] J. Yang, Q.Q. Liu, X.J. Sun, G.F. Xu, X.N. Cheng, Synthesis of negative thermal expansion materials $ZrW_{2-x}Mo_xO_8(0\le x\le 2)$ using hydrothermal method, Ceramics International 35 (2009) 441–445.

[14] H.F. Liu, Z.P. Zhang, W. Zhang, X.B. Chen, Negative thermal expansion ZrW_2O_8 thin films prepared by pulsed laser deposition, Surface and Coatings Technology 205 (2011) 5073–5076.
[15] Z.J. Xiao, X.N. Cheng, X.H. Yan, Effect of post-deposition annealing on ZrW_2O_8 thin films prepared by radio frequency magnetron sputtering, Surface and Coatings Technology 201 (2007) 5560.
[16] H.F. Liu, X.N. Cheng, Z.Z. Zhang, Preparation and properties of negative thermal expansion ZrW_2O_8 thin films deposited by radio frequency magnetron sputtering, Physica Status Solidi B 245 (2008) 2509–2513.
[17] A.H. Farha, A.O. Er, Y. Ufuktepe, G. Myneni, H.E. Elsayed-Ali, Effects of substrate temperature on properties of NbN_x films grown on Nb by pulsed laser deposition, Applied Surface Science 258 (2011) 1613–1618.
[18] G. Shuklaa, P.K. Mishrab, A. Kharea, Effect of annealing and O_2 pressure on structural and optical properties of pulsed laser deposited TiO_2 thin films, Journal of Alloys and Compounds 489 (2010) 246–251.
[19] X.J. Sun, J. Yang, Q.Q. Liu, X.N. Cheng, Influence of sodium dodecyl benzene sulfonate (SDBS) on the morphology and negative thermal expansion property of ZrW_2O_8 powders synthesized by hydrothermal method, Journal of Alloys and Compounds 481 (2009) 668–672.
[20] T. Tsuji, Y. Yamamura, N. Nakajima, Thermodynamic properties of negative thermal expansion materials ZrW_2O_8 substituted for Zr site, Thermochimica Acta 416 (2004) 93–98.
[21] C. Closmann, A.W. Sleight, J.C. Haygorth, Low-temperature synthesis of ZrW_2O_8 and Mo-substituted ZrW_2O_8, Journal of Solid State Chemistry 139 (1998) 424–426.